Non-unit Distance Protection Algorithm for Multiterminal MMC-HVDC Systems Using DC Capacitor Resonance Frequency

Vinícius A. Lacerda, Renato M. Monaro, *Member, IEEE,* Rafael Peña-Alzola, *Senior Member, IEEE,* David Campos-Gaona, *Senior Member, IEEE,* Denis V. Coury

***Abstract*—High-voltage DC (HVDC) transmission has been largely used to interconnect asynchronous systems and integrate renewable energy resources into electrical grids. However, the high short-circuit currents and low-tolerance of power electronics equipment impose new challenges for these systems' protection. To address these challenges, a new distance protection algorithm for HVDC grids with Modular Multilevel Converters (MMCs) is proposed in this paper. The proposed algorithm identifies the faulty line/cable using the resonance frequency of a DC capacitor installed in each terminal. The technique was tested in a four-terminal HVDC grid with five cables and ten circuit breakers. The algorithm was highly selective for faults in the lines and provided fast identification, in less than 1 ms, without communication amongst terminals. The algorithm was tested in hardware under high-noise conditions and provided reliable results.**

***Index Terms*—Distance protection, HVDC, Modular Multilevel Converter (MMC), Protection, Short-circuit.**

I. Introduction

HIGH-Voltage DC (HVDC) transmission has recently been considered the preferred option to interconnect asynchronous systems and integrate renewable energy resources into electrical grids [1]. However, when point-to-point HVDC systems are interconnected forming meshed DC grids, new challenges arise in terms of control, stability and protection [2], [3].

In terms of protection, major challenges are the absence of fault current zero-crossing, the sharp rise of fault currents, the need for fast-breaking time and the high energy absorption requirements of protective elements [4], [5]. To address these challenges, new protection algorithms and DC circuit breaker technologies have been proposed [5]. Although promising fault detection algorithms were proposed, substantial improvements are still required in fault identification, especially concerning selectivity [6].

Several types of primary protection algorithms have been proposed, such as travelling waves [7]–[10], derivative [11]–[13], differential [14], transient [15]–[17] and machine learning-based algorithms [18], [19]. Travelling wave-based algorithms provide high-speed protection, but they have demanding measurement requirements and may increase in complexity in case of high-frequency signals, such as noise, spikes and lightning components associated with multiple reflections within the system. However, recent research has been performed to reduce the sampling frequency of travelling-wave based algorithms [20], [21]. Derivative-based protection algorithms present good selectivity but may be challenging for higher fault resistances associated with noise, and also require high sampling frequencies, accurate measurements, compensation of filter delays and thresholds difficult to define. Similar noise-related issues might be present in methods based on second-order derivatives and the current comparison rate of change, such as [22], [23], although these methods require less pre-defined thresholds. Differential protection techniques are intrinsically selective but require a dedicated communication link and the time delay required to ensure reliable operation may become prohibitive in large systems. Transient-based and machine learning-based protection, despite presenting a good performance, lacks a simpler and straightforward design. Alternative schemes based on distributed optical sensors [24], active pulse injection [25], statistical methods [26], and curve fitting [27] have also been proposed.

Among several protection algorithms for transmission lines/cables, distance protection stands out as it is intrinsically related with the nature of the protected element (protection zones are defined in terms of distance), it has lower measurement-system requirements and does not require communication to operate. However, differently from AC systems, the lack of a fundamental power frequency in DC systems precludes the estimation of impedance and consequently the calculation of the distance to the fault.To circumvent this limitation, alternative distance protection algorithms were proposed for HVDC systems.

The ratio of the voltage drop between two known locations is used in [28] to estimate the fault distance. The technique is fast but was tested for short-cables only. In [29], the differential equations of the protected cable's frequency-dependent model are solved to estimate the distance to the fault in a line-commutated converter (LCC)-HVDC system. The algorithm provided precise estimations, but the large 15 ms window makes it unfeasible for primary HVDC grid protection. The time window was reduced to 4 ms in [30], but, this may still be prohibitive when considering the circuit

V. A. Lacerda is with the Centre d'Innovacio Tecnològica en Convertidors Estatics i Accionaments (CITCEA-UPC), Universitat Politecnica de Catalunya (vinicius.lacerda@upc.edu). R. M. Monaro and D. V. Coury are with the University of São Paulo, Brazil. (monaro@usp.br; coury@sc.usp.br). R. Peña-Alzola and D. Campos-Gaona are with the University of Strathclyde, Glasgow, Scotland. (rafael.pena-alzola@strath.ac.uk; d.campos-gaona@strath.ac.uk).

breaker's opening time. Hence, there is a lack of fast, selective and non-unit distance protection algorithms for HVDC grids.

A new distance protection algorithm for DC grids with Modular Multilevel Converters (MMCs) is proposed in this paper. The proposed algorithm identifies the faulty line/cable using the resonance frequency of a probe capacitor installed in each system's terminal. The contributions of this paper are summarized as follows:

- The algorithm is highly selective for faults in the lines and provides fast fault identification in less than 1 ms;
- The algorithm operates with local measurements only, without communication amongst terminals;
- The algorithm is straightforward and the design procedure was inspired by AC distance protection, which makes it attractive to protection engineers;
- The algorithm was tested in hardware under high-noise conditions and provided reliable results.

The remainder of this paper is organized as follows. Section II presents the proposed distance protection algorithm and the short-circuit theory associated to it. The algorithm performance is evaluated using simulations presented in Section III. The real-time tests in hardware are shown in Section IV. Finally, the conclusions are drawn in Section V.

II. Proposed Protection Algorithm

The proposed protection algorithm is based on the estimation of the resonance frequency of a probe capacitor installed in each system terminal. The capacitor is connected between the DC poles and the ground (some studies also considered the presence of a DC capacitor to provide a reference to the ground in the DC side [6], [31]–[33]). In a steady-state condition, each capacitor will be charged at a half nominal voltage ($V_{dc}/2$). When a DC fault happens, the interaction between the probe capacitor and the line/cable inductance will produce an oscillation at a natural frequency that depends on the capacitor size and the total inductance to the fault. As the line/cable inductance is dependent on the conductor length, a relationship between resonance frequency and the distance to the fault can be established, similar to what it is done for AC grid distance protection. The proposed protection scheme is illustrated in Fig. 1.

The protection algorithm comprises three parts: i) the fault detection that detects any fault in the DC grid, regardless of its location, ii) the fault classification that classifies the fault as pole-to-pole (PP) or pole-to-ground (PG) and iii) the fault identification, which is the main scope of this paper and identifies in which cable/line (protection zone) the fault has occurred. In this study, we have used the algorithms shown in Section II.E for fault detection and classification and the distance protection described in this section for fault identification. Additional modules such as a directional module based on the polarity of the current derivative can also be added, which is useful to detect busbar faults.

A. Fault analysis with the DC probe capacitor

The MMC fault analysis is commonly divided into three stages [34], [35]. The first is the capacitive discharge stage,

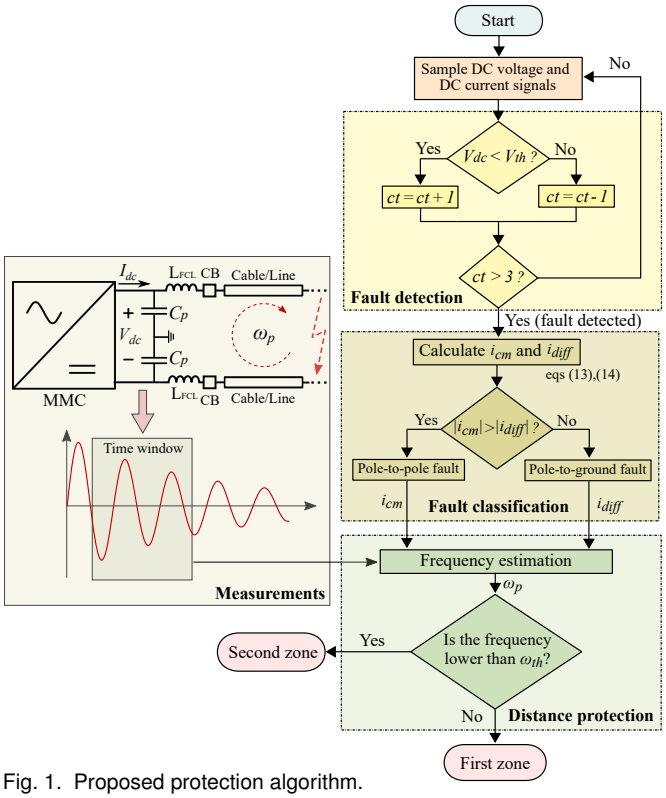

Fig. 1. Proposed protection algorithm.

which is the period between the fault inception and the blocking of the converter. After the converter is blocked, the AC transient infeed stage starts, in which the energy stored in the converter arm inductors is released into the fault. After the inductors discharge the stored energy, the fault is fed by the AC grid in the AC steady-state infeed stage. The proposed protection is designed to operate with maximum accuracy in the first fault stage, before the converter is blocked.

To simplify the expressions, only the terminal connected to the circuit breaker under analysis was represented for both PP and PG faults. Fault analyses that consider more elements in the system can be found in [36]–[38].

1) Pole-to-pole faults: The equivalent circuit of the system with the DC probe capacitor, in a PP fault is shown in Fig. 2.

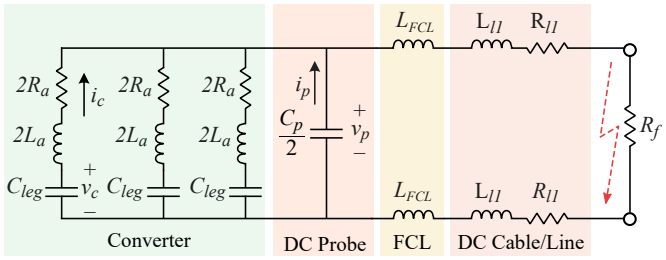

Fig. 2. PP fault equivalent circuit considering the DC probe capacitor.

Where C_{leg} is the equivalent capacitance between positive and negative arms, L_a is the arm inductance, R_a represents the arm losses, C_p is the DC probe capacitance, L_{FCL} is the DC fault current limiter inductance, R_f is the fault resistance and L_l1 and R_l1 are the equivalent line/cable inductance and resistance up to the fault spot, respectively.

It is convenient to define equivalent parameters for the circuit in Fig. 2 to reduce the size of the system's Ordinary

Differential Equations (ODEs):

$$\begin{cases} R_{dc1} = R_{l1} + R_f/2 \\ L_{dc1} = L_{FCL} + L_{l1} \end{cases} \tag{1}$$

Using the equivalent parameters and applying Kirchhoff's voltage and current laws (KVL and KCL) to the circuit results in the following system of ODEs:

$$\frac{\mathrm{d}i_c}{\mathrm{d}t} = \frac{v_c - v_b}{2L_a} - \frac{R_a}{L_a} i_c \tag{2a}$$

$$\frac{\mathrm{d}v_c}{\mathrm{d}t} = -\frac{1}{C_{leg}} i_c \tag{2b}$$

$$\frac{\mathrm{d}i_p}{\mathrm{d}t} = 3i_c\left(\frac{R_a}{L_a} - \frac{R_{dc1}}{L_{dc1}}\right) + \frac{v_p}{2}\left(\frac{3}{L_a} + \frac{1}{L_{dc1}}\right) - \frac{3v_c}{2L_a} - \frac{R_{dc1}}{L_{dc1}} i_p \tag{2c}$$

$$\frac{\mathrm{d}v_p}{\mathrm{d}t} = -\frac{2}{C_p} i_p \tag{2d}$$

As (2) is linear, the system has a unique solution. Nevertheless, obtaining an exact closed-form solution involves calculating the roots of a fourth-order polynomial, which produces lengthy expressions. However, the desired resonance frequency between C_p and the system can be obtained from the system poles, in the frequency domain, using the Laplace transform. For the Laplace transform, without loosing generality, the following initial conditions are used: $i_c(0) = I_{dc}/3$, $v_c(0) = V_{dc}$, $i_p(0) = 0$ and $v_p(0) = V_{dc}$. These initial conditions represent the DC side circuit in steady state (C_{leg} and C_p fully charged and constant DC voltage equal V_{dc}) for a given power flow determined by I_{dc}. To simplify this, we consider $I_{dc} = 0$, as it does not influence the resonance frequency. Thus, we have the following for the current i_p:

$$I_p(s) = \frac{\frac{V_{dc}}{2L_{dc}\omega_c^2\omega_p^2}s^2 + C_pC_{leg}R_aV_{dc}s + C_pV_{dc}}{P(s)} \tag{3}$$

where s is the Laplace variable and

$$P(s) = 1 + \frac{2}{\tau\omega_c^2}s + \frac{1}{\omega_c^2}s^2 + \frac{2}{\tau_{eq}\omega_c^2\omega_p^2}s^3 + \frac{1}{\omega_c^2\omega_p^2}s^4 \tag{4}$$

where

$$\omega_c = \sqrt{\frac{1}{L_{eq}C_{leg}}} \tag{5}$$

$$\omega_p = \sqrt{\frac{L_{eq}}{2C_pL_aL_{dc1}}} \tag{6}$$

are the system undamped resonance frequencies, and

$$\tau = \frac{2L_{eq}}{R_{eq}} \tag{7}$$

$$\tau_{eq} = \left(\frac{R_{dc1}}{2L_{dc1}} + \frac{R_a}{2L_a}\right)^{-1} \tag{8}$$

are the system time constants, that provide exponential decay. They are calculated using the equivalent parameters:

$$\begin{cases} L_{eq} = 2L_a + 6L_{dc1} + L_{dc1}C_p/C_{leg} + 2C_pR_aR_{dc1} \\ R_{eq} = 2R_a + 6R_{dc1} + R_{dc1}C_p/C_{leg} \end{cases} \tag{9}$$

The resonance frequency associated with C_p (ω_p) varies with the distance as both L_{eq} and L_{dc1} increase with the distance to the fault. Thus, the distance to the fault can be related to ω_p. Additionally, as the time constants are influenced by the fault resistance and the line parameters are known, it is even possible to estimate the fault resistance if the exponential decay is correctly calculated. However, as the purpose of the fault distance algorithm is to identify the faulty line/cable, we leave the estimation of other parameters to dedicated algorithms, such as fault location algorithms.

The voltage $v_p(t)$ can be obtained from i_p using (2d) or its equivalent in the frequency domain. As the system poles are the same, both $v_p(t)$ and $i_p(t)$ can be used to estimate ω_{p0}. However, as $i_p(0) = 0$ and i_p is the derivative of v_p, i_p is less affected by the DC offset, thus being preferred to estimate the resonance frequency.

2) Pole-to-ground faults: The equivalent circuit of the system with the DC probe capacitor, in a PG fault is shown in Fig. 3.

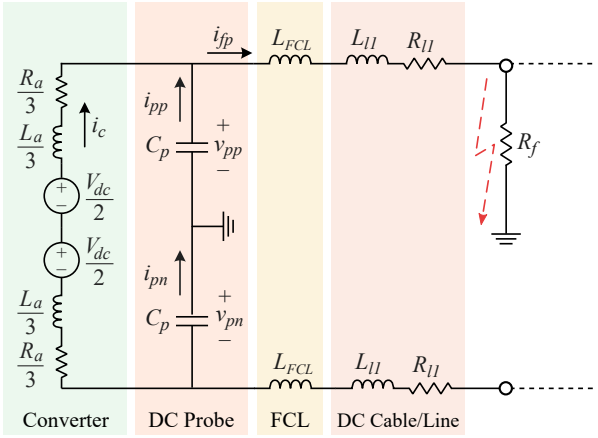

Fig. 3. Pole-to-ground fault equivalent circuit considering the DC probe capacitor.

Similarly to what was developed for the PP fault case, the first step to find the resonance frequency is to find the expression for the system poles in the frequency domain, using the Laplace transform. Afterwards, the resonance frequencies are obtained from the system poles. Finally, the resonance frequency associated with C_p is identified, as follows.

$$\omega_p = \sqrt{\frac{1}{2C_p}\left(\frac{3}{L_a} + \frac{1}{L_{dc1}} + \frac{1}{L_{dc}} + \sqrt{\left(\frac{L_{dc2}}{L_{dc}L_{dc1}}\right)^2 + \left(\frac{3}{L_a}\right)^2}\right)} \tag{10}$$

where $L_{dc} = L_{dc1} + L_{dc2}$ and L_{dc2} is the inductance of the cable/line between the fault and the opposite terminal. The other parameters are the same as the PP fault ones.

Similarly to the PP fault, here the resonance frequency associated with C_p (ω_p) also varies with the distance to the fault as L_{dc1} increases with distance. Thus, the distance to the fault is also related to ω_p calculated for the PG fault.

It should be noted that although the variable used for the resonance frequency ω_p is the same as in (6) and (10), its expression is different. Thus, the fault must be previously classified in PP or PG before selecting the appropriate expression. The expressions for the resonance frequencies do

not consider the system losses and the fault resistance because these variables have minor influence on the final frequency value. Moreover, only the total capacitance of the converter is used, which does not change during the fault.

From the derivation presented, it can be observed that the proposed protection algorithm only requires information about the converter and DC reactor parameters, which are readily available by the manufacturer. This allows a simple and straightforward setup for the proposed technique.

B. Protection zones

Defining appropriate protection zones is key to ensuring that the protection system will be selective. In AC systems, the first protection zone is commonly defined between 80% and 90% of the protected line length, providing an underreaching zone [39], [40]. The second protection zone is set to overreach the protected line, typically between 120% and 150% of the protected line length [39], [40]. An underreaching zone is set to considerate uncertainties and avoid instantaneous operation for a fault on the other line.

However, as in VSC-HVDC systems, DC reactors (L_{FCL}) are inserted to limit the fault current, these reactors also provide a big step of inductance at the line ends. As a result, the resonance frequency steeply decreases when a fault happens on the adjacent line. Thus, differently from AC distance protection, the proposed DC distance protection can have a reach of 100% for the first protection zone. Fig. 4 illustrates how the resonance frequency drops between the protected line and the adjacent line. If the rating of the DC reactor is reduced, the electric boundary between adjacent lines will decrease. This will not impede using the protection algorithm but will reduce its reach.

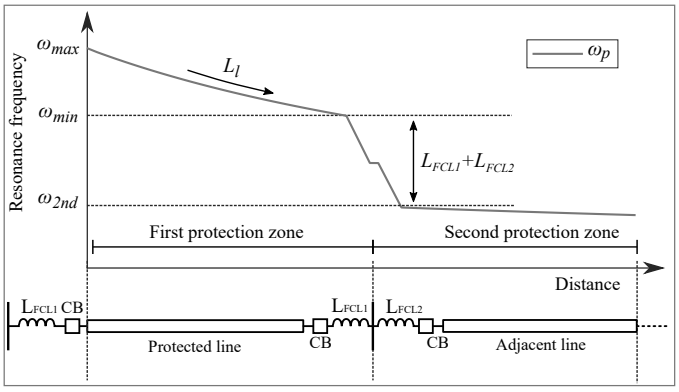

Fig. 4. Illustration of how the resonance frequency varies between first and second protection zones.

Fig. 4 shows that the threshold frequency (ω_{th}), which is used to discriminate a fault as in the first or second protection zones, can be chose between ω_{min} and ω_{2nd}:

$$\omega_{2nd} < \omega_{th} < \omega_{min} \tag{11}$$

However, as the travelling waves corrupt the frequency estimation with high-frequency components, the estimated resonance frequency might be higher than the analytical value, depending on the frequency estimation technique used. In this case, (11) can be used as a starting point and the final ω_{th} can be defined using the simulated fault signals and considering measurement errors.

C. Sizing the DC probe capacitor

As (6) and (10) show, ω_p is totally dependent on the DC probe capacitance (C_p). If a big capacitance value is chosen, the ω_p will be low and the signal processing algorithm responsible for estimating the resonance frequency will need a wider time window to provide a reliable frequency estimation, thus reducing the algorithm speed. However, if the capacitance is chosen too small, it might be associated with the system parasitic capacitance, corrupting the i_p waveform. Therefore, C_p should be large enough to not be associated with the system parasitic capacitance but should be small enough to provide a high-frequency discharge during a fault. A good starting point would be to select C_p such that:

$$\omega_p < \frac{2\pi}{t_{tw}} \tag{12}$$

where, t_{tw} is the time it takes the waves to travel along the full length of the protected cable. This generally implies in a capacitor one order of magnitude smaller than the converter capacitance, as shown in Section III-A. However, this in practice will be an engineering decision tailored for each system.

D. Measured variables

Both C_p voltages and currents can be used to estimate the resonance frequency. However, the currents (i_{pp} and i_{pn}) were used as they are approximately equal to zero before the fault and consequently require less DC filtering. The common-mode current i_{cm} was used for PP faults and the differential current i_{diff} was used for PG faults, as follows:

$$i_{cm} = \frac{i_{pp} + i_{pn}}{2} \tag{13}$$

$$i_{diff} = i_{pp} - i_{pn} \tag{14}$$

Any signal processing algorithm capable of providing a reliable frequency estimation [41], [42] can be used in the proposed distance protection, such as Discrete Fourier Transform (DFT), Least Mean Squares (LMS), Wavelet transform, Stockwell transform, ESPRIT, MUSIC, among others. In this work, the LMS was used, following the first method described in [43], due to its simplicity and precision.

E. Fault detection and classification

The fault detection is performed by an undervoltage algorithm:

$$V_{dc} < V_{th} \tag{15}$$

where V_{dc} is the measured terminal DC voltage after filtering and V_{th} is the undervoltage threshold, equal to 0.85 p.u in this study.

A counter is incremented if (15) is true and decremented if it is false. When the counter reaches 3, the fault is detected. This avoids misdetection due to noise and spikes.

The fault classification is performed by comparing the currents in the positive and the negative poles, using the currents described in (13) and (14). When the fault is PG, the current in the faulty pole will be higher than the current in the healthy pole; hence i_{diff} will be high. When the fault is PP, the currents in both poles will be approximately equal; hence i_{diff} will be close to zero and i_{cm} will be high. Therefore, the fault is classified as a PP one if $|i_{cm}| > |i_{diff}|$. Conversely, the fault is classified as a PG one if $|i_{diff}| > |i_{cm}|$.

III. Simulation Results

In this section, the protection performance is analysed in a simulation environment.

A. Test system and methodology

In order to evaluate the proposed algorithm, the symmetrical monopolar, four-terminal system presented in Fig. 5, based on [44], was simulated in PSCAD/EMTDC. The converters were modeled with the detailed Thévenin equivalent model [45]. All DC links were modeled using the frequency-dependent cable model. The cables were 320 kV cross-linked polyethylene (XLPE) insulated and their parameters were based on [44]. The armour and sheath were assumed to be ideally grounded, and soil resistivity was assumed to be 1 Ωm. The converter's internal overcurrent protection was set to 2 p.u. = 3.87 kA for MMC 4 and equal to 2.9 kA for MMCs 1, 2 and 3. The pick-up time was 100 μs. $L_{FCL} = 30$ mH in the terminals 1, 2 and 3 and equal to 50 mH in the terminal 4.

All voltages and currents were corrupted with white noise with SNR = 40 dB. The DC component due to pole unbalance was filtered from the currents in C_p using a 2-order high-pass Butterworth filter with cutting frequency of 50 Hz. No low-pass filtering was necessary due to the noise-tolerant characteristic of the LMS. For the terminal voltages, a moving average filter was used with a length equal to 4 samples. All variables were processed at a sampling frequency of 50 kHz. The LMS parameters were: window length $L = 35$ samples and distance between consecutive samples $k = 12$.

The proposed protection algorithm was tested in all ten circuit breakers of the system, at the same time. The breakers were called CB_{xy}, where x was the terminal where the breaker was installed and y the far terminal where the protected line was connected.

As the same DC capacitor provides measurement for all circuit breakers in a terminal, only one breaker per terminal should proceed to fault identification. Thus, the fault identification was performed only for the first breaker of each terminal to detect the fault by undervoltage. This requires communication between circuit breakers within the same terminal, but can also be performed locally in the breaker by detecting a negative current derivative [23], [46]. Using the polarity of the current derivative can also discriminate busbar faults, although the full consideration of these faults was not within our scope. The beginning of the time window for the frequency estimation was defined as five samples before i_{cm} or i_{diff} reached 0.04 kA.

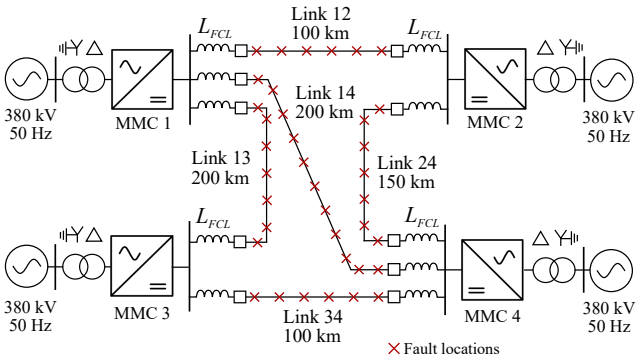

Fig. 5. HVDC test system [44] used for the algorithm evaluation.

TABLE I
Defined protection thresholds for fault identification

ω_{th}	Terminal 1			Terminal 2		Terminal 3		Terminal 4		
(Hz)	CB_{12}	CB_{13}	CB_{14}	CB_{21}	CB_{24}	CB_{31}	CB_{34}	CB_{41}	CB_{42}	CB_{43}
PP	960	880	880	870	840	810	840	750	810	840
PG	760	740	740	690	670	660	680	620	640	660

1) Simulated faults: PP and positive PG faults were simulated from the beginning to the end of all cables, in steps of 10 km. The simulated fault resistances were 1 Ω, 10 Ω, 30 Ω, 50 Ω and 80 Ω. In total, 700 faults were simulated. The circuit breakers operation was not considered in the simulations, only their measurements and trip signals. Further details on their operation can be found in [47].

2) Sizing the DC probe capacitors: The simulated cable travelling wave speed was 183.5 km/ms, which resulted in a maximum travel time of 200 km/183.5 km/ms = 1.09 ms in the longest cable. Thus, C_p was chosen such that the inverse of the minimum resonance frequency ($1/\omega_{min}$) in the first zone was lower than this maximum travel time. Because of the skin effect, the cable parameters change with frequency, hence the resistance and inductance must be calculated at the desired resonance frequency. At 800 Hz the cables' total inductance was: $L_{12} = 21.2$ mH, $L_{13} = 42.3$ mH, $L_{14} = 42.3$ mH, $L_{24} = 31.7$ mH, $L_{34} = 21.2$ mH. Although the cables' inductance varies with frequency, this variation is more significant in a log-scale, where the frequencies vary thousands of times compared to the nominal value. In the case of this study, all analyzed frequencies have the same order of magnitude and, when summed with the fixed inductance of the DC reactor, their variation around ω_{min} was negligible. For the sake of simplicity, a common $C_p = 2\,\mu$F was chosen for all terminals, which respects the maximum travel time aforementioned.

3) Defining the thresholds: According to Fig. 4, any threshold between ω_{min} and ω_{2nd}, calculated by the analytical model, would ensure selectivity between the two zones. However, the reflection of the travelling waves on the terminal has a high-frequency content which corrupts the frequency estimation, raising the estimated frequency. Therefore, the analytical model (6) and (10) was used as a starting point and the threshold is adjusted to a value between ω_{min} and ω_{2nd} obtained from the simulations. The defined frequency thresholds, in Hz, are summarized in Table I.

TABLE II
PROPOSED PROTECTION SELECTIVITY

	Terminal 1			Terminal 2		Terminal 3		Terminal 4		
R_f	CB_{12}	CB_{13}	CB_{14}	CB_{21}	CB_{24}	CB_{31}	CB_{34}	CB_{41}	CB_{42}	CB_{43}
1 Ω	100%	100%	100%	100%	100%	100%	100%	100%	100%	100%
10 Ω	100%	100%	100%	100%	100%	100%	100%	100%	100%	100%
30 Ω	100%	100%	100%	100%	100%	100%	100%	100%	100%	100%
50 Ω	100%	100%	100%	99.3%	98.6%	98.6%	98.6%	100%	100%	98.6%
80 Ω	99.3%	100%	100%	98.6%	98.6%	97.9%	97.9%	99.3%	99.3%	98.6%

B. Results overview

For all simulated faults up to 30 Ω, distance protection operated with 100% of selectivity, correctly identifying a fault as being in the first or second zone. It should be noted that this result was observed in all ten circuit breakers at the same time, totaling almost 7000 corrected operations. The overall result is shown in Table II. As can be observed in Table II, the proposed protection technique was also highly selective for higher fault resistances, such as 50 Ω and 80 Ω. The proposed algorithm presented high selectivity even using lower values for L_{FCL} than described by [5].

C. Test cases

To exemplify the proposed distance protection, two cases are discussed in more detail: a 30 Ω PP fault on Link 14, 150 km from MMC 4 and a 1 Ω PG fault on Link 12, 70 km from MMC 1. In both tests, t_b indicates the beginning of the time window and L the window length.

1) PP fault 150 km from MMC 4: Fig. 6 shows the positive pole voltage V_{dcp}, i_{cm} and ω_p for the first fault case, measured by CB_{41}. Although the fault happened at $t=0$, it took 0.8 ms to hit the Terminal 4 (T4). Following the fault inception, C_p oscillates and the resonance frequency is estimated. The protection trips for all breakers are shown in Fig. 7. As can be observed in Fig. 7, all breakers correctly detected the fault. The different detection delays among breakers was because the travelling waves take a longer time to reach distant terminals. Although all breakers detected the fault, only one breaker per terminal proceeded with the fault identification algorithm, with CB_{14} and CB_{41} correctly identifying the fault as in the first zone and CB_{21} and CB_{31} correctly identifying the fault as in the second zone.

2) PG fault 70 km from MMC 1: Fig. 8 shows V_{dcp}, i_{diff} and ω_p for the second fault case. In this fault case, the converter was blocked at $t=1.9$ ms, which changed the resonance frequency. However, as the frequency was already estimated, the blocking of the converter did not influence the protection performance. The protection trips for all breakers are shown in Fig. 9. As can be observed in Fig. 9, all breakers detected the fault. The fault identification was performed correctly, with CB_{12} and CB_{21} identifying the fault as in the first zone and CB_{31} and CB_{42} identifying the fault as in the second zone.

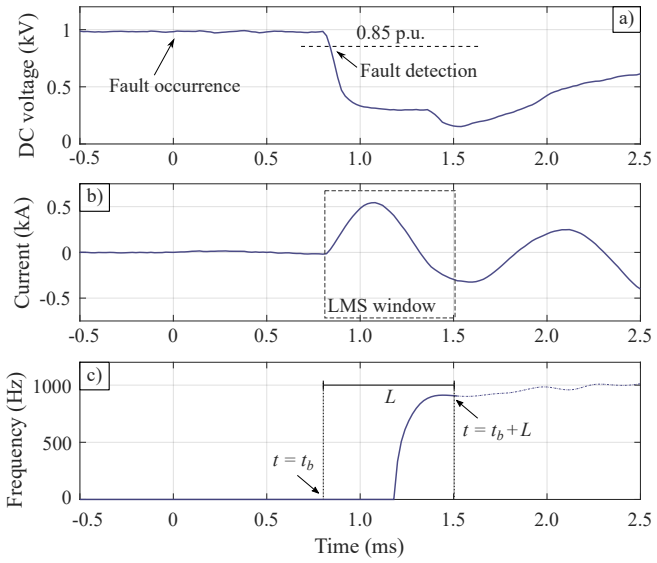

Fig. 6. 30 Ω PP fault on Link 14, 150 km from MMC 4. Measurements from CB_{41}. a) V_{dcp}. b) i_{cm}. c) Estimated frequency.

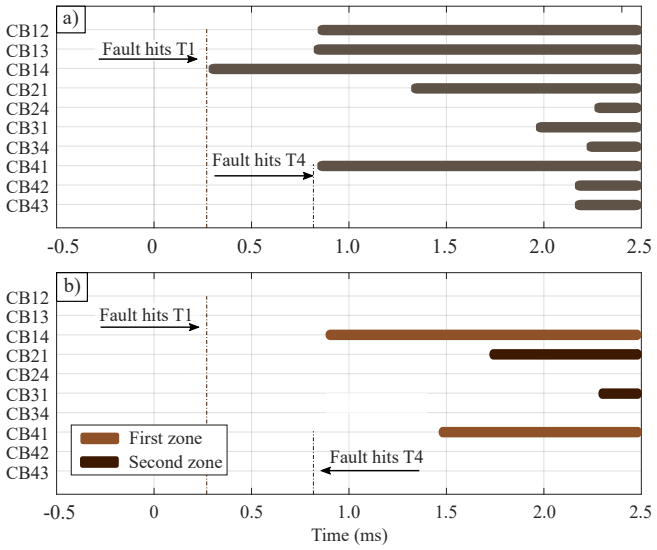

Fig. 7. 30 Ω PP fault on Link 14, 150 km from MMC 4. a) Fault detection states. b) Fault identification states.

D. Influence of converter blocking

The proposed protection algorithm was developed based on the assumption that the converter will be in the capacitive discharge stage (converter no blocked) when ω_p is estimated. As the proposed protection algorithm operates in 700 μs, it is unlikely to have the converter blocked within this period. In all 7000 cases tested, frequency estimation was performed before the converters were blocked. For the most severe scenario (1 Ω PP fault close to the converters) the converters were blocked only after 1.52 ms, which provides a sufficient time-span for frequency estimation. Therefore, in all 7000 cases tested, all frequency estimations were performed before the converters were blocked.

IV. HARDWARE REAL-TIME TESTING

In order to verify the applicability of the proposed technique, the fault identification algorithm was embedded

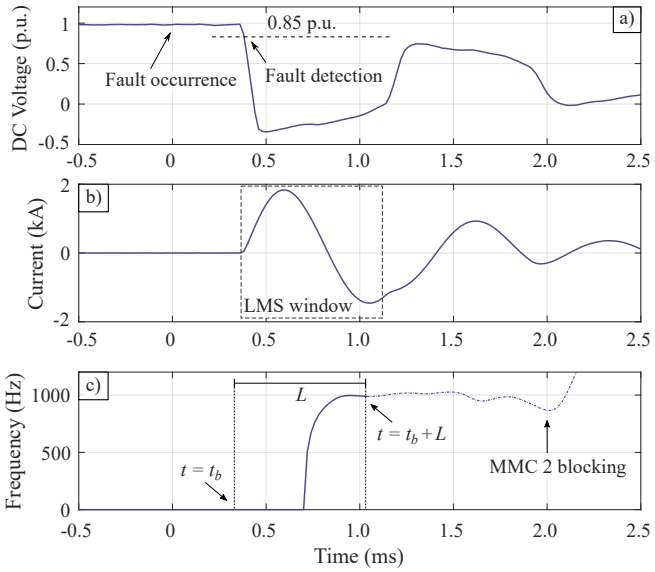

Fig. 8. $1\,\Omega$ PG fault on Link 12, 70 km from MMC 1. Measurements from CB_{12}. a) V_{dcp} b) i_{diff} c) Estimated frequency.

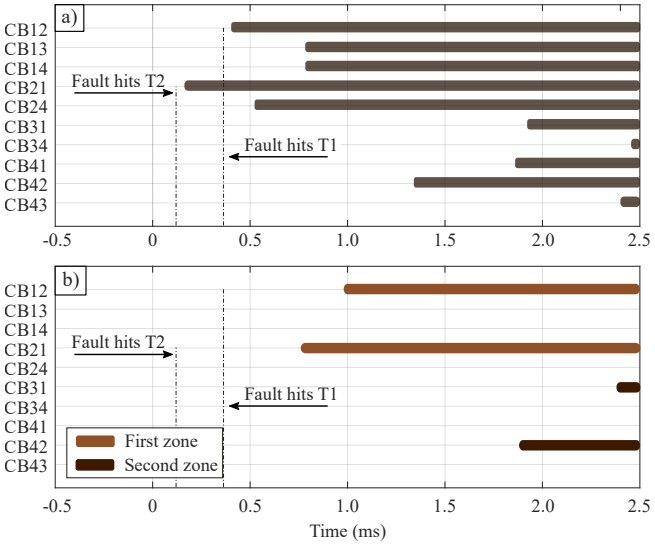

Fig. 9. $1\,\Omega$ PG fault on Link 12, 70 km from MMC 1. a) Fault detection states. b) Fault identification states.

and tested in hardware running in real-time. The algorithm was embedded in four Texas Instruments Microcontroller Unit (MCU) F28379D Launchpad. Each MCU represented one circuit breaker of the four-terminal system. The algorithm ran at a sampling frequency of 50 kHz.

A. Experimental setup

The current waveforms (i_{diff} and i_{cm}) obtained from PSCAD were loaded in the RTDS and then injected into the four MCUs. The waveforms were converted to analog voltage signals between 0–3 V using the following scale: -1.65 kA $\equiv$ 0 V and 1.65 kA $\equiv$ 3 V. Due to intense electromagnetic interference within the laboratory, 8 passive first-order anti-aliasing filters were built. The filter parameters were: $R = 220\,\Omega$, $C = 0.680$ μF and cut-off frequency equal to 1063 Hz. After the analog-to-digital conversion, the currents were filtered by a moving average filter of 18 samples. Four digital states were produced by each MCU: fault detection, estimated frequency (a pulse with a period equal to 5 μs per Hz), first zone trigger and second zone trigger. The digital states were injected back in the RTDS, closing the loop. Thus, a total of 8 analog signals and 16 digital signals were used in the tests. The experimental setup is shown in Fig. 10.

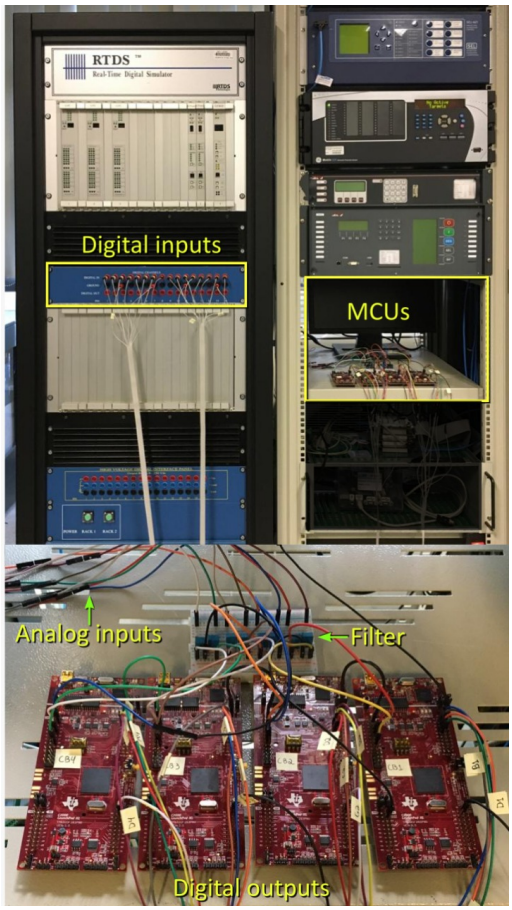

Fig. 10. Experimental setup.

B. Experimental results

The protection for two faults cases is presented. The first case was a $10\,\Omega$ PG fault on Link 34, 40 km from MMC 3. For the first case, the thresholds of the breakers CB_{13}, CB_{24}, CB_{34} and CB_{43} were set. The second case was a $10\,\Omega$ PP fault on Link 24, 70 km from MMC 4. For the second case, the thresholds of the breakers CB_{12}, CB_{24}, CB_{34} and CB_{42} were set. The tests started at $t = 40$ ms with 1 ms of pre-fault. Fig 11 and Fig. 12 show the results for the first and second case, respectively. The proposed algorithm performed correctly in the four emulated circuit breakers and for both fault cases. Only the breakers protecting the faulty cable raised the first zone trip. The delays in fault detection are due to fault waves travel time, as a unique time reference was used for all measurements. The results confirm that the proposed algorithm is not only selective and fast but simple enough to be embedded in a simple MCU, thus not requiring powerful measurement systems and sophisticated signal processing techniques to operate correctly.

This article has been accepted for publication in IEEE Transactions on Industrial Electronics. This is the author's version which has not been fully edited and content may change prior to final publication. Citation information: DOI 10.1109/TIE.2021.3139245

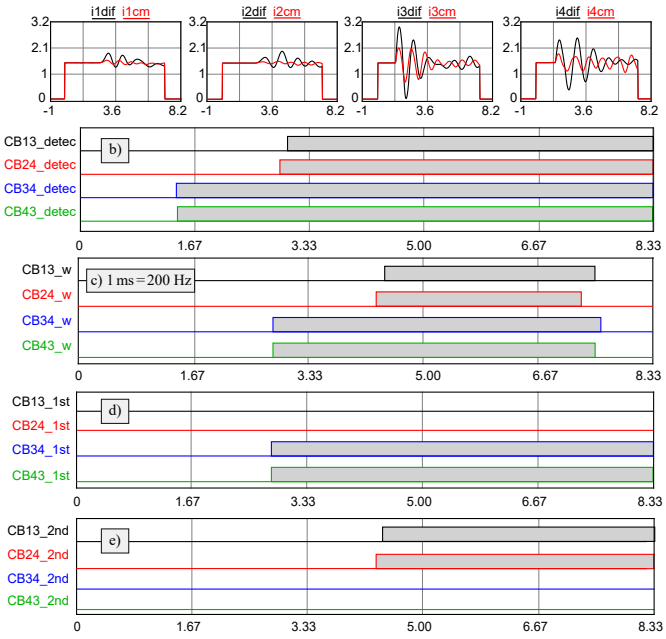

Fig. 11. Hardware test 1 - $10\,\Omega$ PG fault on Link 34, 40 km from MMC 3. a) Current waveforms. b) Fault detection; c) Estimated frequency; d) First zone trip; e) Second zone trip.

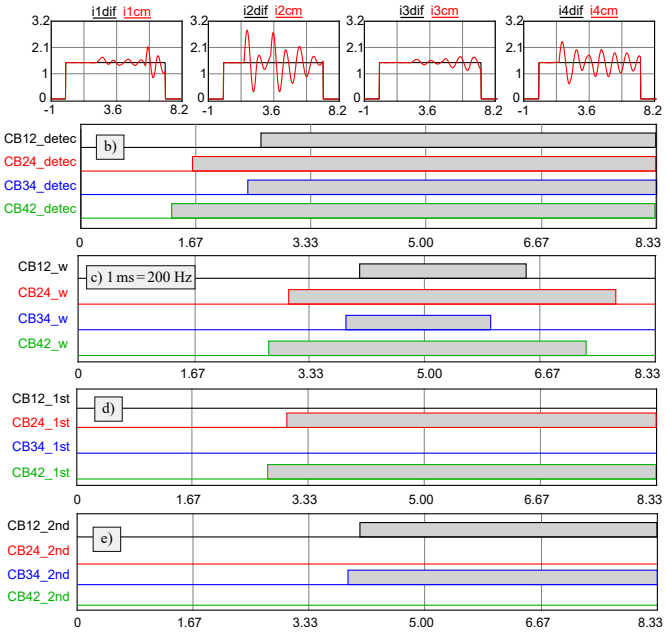

Fig. 12. Hardware test 2 - $10\,\Omega$ PP fault on Link 24, 70 km from MMC 4. a) Current waveforms. b) Fault detection; c) Estimated frequency; d) First zone trip; e) Second zone trip.

C. Practical limitations

The following challenges should be addressed when using the algorithm in real systems:

- Inaccurate system data. During the long-term operation of the HVDC system, parameters such as capacitances and inductances might slightly deviate from the pre-commissioned values due to ageing and degradation. These should be regularly updated to keep the distance estimation at maximum precision.
- Signal processing limitations. The proposed algorithm is based on the estimation of a resonant frequency. Thus, the measurement system and the relay must be capable of adequately filtering and rejecting noise, spikes, and other spurious components in the signal that might affect the frequency estimation. Moreover, the filtering must be well adjusted not to attenuate the resonant frequency component.
- Short lines. If a small DC reactor is used along short transmission lines, the natural frequency of travelling waves can interfere with the resonant frequency. In this situation, the small system must be simulated to verify if the frequency of the travelling waves is too close to the resonant frequency.
- Transient response of instrument voltage and current transformers. The frequency response of the measurement system must be evaluated to avoid spurious oscillations from being generated in the measured currents and voltages.
- Mid-point ground missing. If the system loses the mid-point ground, the poles can be unevenly charged. In the case of a PP fault, the behaviour of the oscillatory component will not change as the equivalent circuit in a PP fault is not affected by the ground. Thus, distance protection will operate normally. However, in the case of a PG fault, as there is no path for the fault current, the oscillatory component will be affected and may even be absent depending on the grounding of the converter. In this scenario, as the common-mode current will always be equal to the differential-mode current, the fault classification will not function properly. However, this can be easily detected by an neutral alarm.

V. Conclusions

The paper proposed a new distance protection algorithm for HVDC grids. The proposed algorithm was capable of providing selective fault identification with local measurements only, using the resonance frequency of a probe capacitor installed in each system terminal. The method is simple, reliable and the design procedure was inspired in AC distance protection, which makes it more attractive to protection engineers.

The proposed algorithm was tested in a four-terminal HVDC grid with five cables and ten circuit breakers operating at the same time, confirming that the same design procedure could be generalized for all circuit breakers. Real-time testing in hardware demonstrated that the algorithm is feasible and simple enough to be embedded in an MCU, thus not requiring powerful measurement systems or sophisticated signal processing techniques to operate correctly.

The proposed technique contributes to the recent efforts to provide a selective, non-unit and fast fault identification in HVDC grids protection. Overcoming these challenges is key to increasing the reliability and availability of future grids.

Future works might address both short-circuit models and protection algorithms. In short-circuit models, research activity is needed to provide more precise representations of DC lines and cables, model the travelling waves with more simplicity, account for the participation of multiple cables

into the fault, and represent the impact of DC faults on the AC side. Moreover, future models should consider a grid composed of different converter topologies. In protection, new investigations can include the fault identification algorithm's performance in an MTDC system comprising different converter topologies, and further tests should be performed with respect to another system's conditions, such as initialization, reconfiguration, line energization, faults produced by lightning, and faults at the DC bus. Another line of research could investigate the use of the proposed distance protection algorithm in medium-voltage DC grids.

REFERENCES

[1] D. V. Hertem, O. Gomis-Bellmunt, and J. Liang, Eds., *HVDC Grids*. John Wiley & Sons, Inc., Feb. 2016.

[2] D. Jovcic and K. Ahmed, *High voltage direct current transmission: converters, systems and DC grids*. John Wiley & Sons, 2015.

[3] N. R. Chaudhuri, R. Majumder, B. Chaudhuri, and J. Pan, "Stability analysis of VSC MTDC grids connected to multimachine AC systems," *IEEE Transactions on Power Delivery*, vol. 26, DOI 10.1109/tpwrd.2011.2165735, no. 4, pp. 2774–2784, Oct. 2011.

[4] A. Shukla and G. D. Demetriades, "A survey on hybrid circuit-breaker topologies," *IEEE Transactions on Power Delivery*, vol. 30, DOI 10.1109/tpwrd.2014.2331696, no. 2, pp. 627–641, Apr. 2015.

[5] D. Jovcic, G. Tang, and H. Pang, "Adopting circuit breakers for high-voltage DC networks: Appropriating the vast advantages of DC transmission grids," *IEEE Power and Energy Magazine*, vol. 17, DOI 10.1109/mpe.2019.2897408, no. 3, pp. 82–93, May. 2019.

[6] CIGRE Working Group B4-52, *Technical Brochure 533: HVDC Grid Feasibility Study*. CIGRE, 2013.

[7] Y. Li, Y. Gong, and B. Jiang, "A novel traveling-wave-based directional protection scheme for MTDC grid with inductive DC terminal," *Electric Power Systems Research*, vol. 157, DOI 10.1016/j.epsr.2017.12.010, pp. 83–92, Apr. 2018.

[8] G. Zou, Q. Feng, Q. Huang, C. Sun, and H. Gao, "A fast protection scheme for VSC based multi-terminal DC grid," *International Journal of Electrical Power & Energy Systems*, vol. 98, DOI 10.1016/j.ijepes.2017.12.022, pp. 307–314, Jun. 2018.

[9] X. Pei, H. Pang, Y. Li, L. Chen, X. Ding, and G. Tang, "A novel ultra-high-speed traveling-wave protection principle for VSC-based DC grids," *IEEE Access*, vol. 7, DOI 10.1109/access.2019.2936276, pp. 119 765–119 773, 2019.

[10] C. Zhang, G. Song, T. Wang, L. Wu, and L. Yang, "Non-unit traveling wave protection of HVDC grids using levenberg–marquart optimal approximation," *IEEE Transactions on Power Delivery*, vol. 35, DOI 10.1109/tpwrd.2020.2964717, no. 5, pp. 2260–2271, Oct. 2020.

[11] W. Leterme, J. Beerten, and D. V. Hertem, "Nonunit protection of HVDC grids with inductive DC cable termination," *IEEE Transactions on Power Delivery*, vol. 31, DOI 10.1109/tpwrd.2015.2422145, no. 2, pp. 820–828, Apr. 2016.

[12] J. Sneath and A. D. Rajapakse, "Fault detection and interruption in an earthed HVDC grid using ROCOV and hybrid DC breakers," *IEEE Transactions on Power Delivery*, vol. 31, DOI 10.1109/tpwrd.2014.2364547, no. 3, pp. 973–981, Jun. 2016.

[13] C. Li, A. M. Gole, and C. Zhao, "A fast DC fault detection method using DC reactor voltages in HVdc grids," *IEEE Transactions on Power Delivery*, vol. 33, DOI 10.1109/tpwrd.2018.2825779, no. 5, pp. 2254–2264, Oct. 2018.

[14] A. E. Abu-Elanien, A. A. Elserougi, A. S. Abdel-Khalik, A. M. Massoud, and S. Ahmed, "A differential protection technique for multi-terminal HVDC," *Electric Power Systems Research*, vol. 130, DOI 10.1016/j.epsr.2015.08.021, pp. 78–88, Jan. 2016.

[15] J. Liu, N. Tai, and C. Fan, "Transient-voltage-based protection scheme for DC line faults in the multiterminal VSC-HVDC system," *IEEE Transactions on Power Delivery*, vol. 32, DOI 10.1109/tpwrd.2016.2608986, no. 3, pp. 1483–1494, Jun. 2017.

[16] Y. Li, L. Wu, J. Li, L. Xiong, X. Zhang, G. Song, and Z. Xu, "DC fault detection in MTDC systems based on transient high frequency of current," *IEEE Transactions on Power Delivery*, vol. 34, DOI 10.1109/tpwrd.2018.2882431, no. 3, pp. 950–962, Jun. 2019.

[17] W. Xiang, S. Yang, L. Xu, J. Zhang, W. Lin, and J. Wen, "A transient voltage-based DC fault line protection scheme for MMC-based DC grid embedding DC breakers," *IEEE Transactions on Power Delivery*, vol. 34, DOI 10.1109/tpwrd.2018.2874817, no. 1, pp. 334–345, Feb. 2019.

[18] Q. Yang, S. L. Blond, R. Aggarwal, Y. Wang, and J. Li, "New ANN method for multi-terminal HVDC protection relaying," *Electric Power Systems Research*, vol. 148, DOI 10.1016/j.epsr.2017.03.024, pp. 192–201, Jul. 2017.

[19] R. Bertho, V. A. Lacerda, R. M. Monaro, J. C. M. Vieira, and D. V. Coury, "Selective nonunit protection technique for multiterminal VSC-HVDC grids," *IEEE Transactions on Power Delivery*, vol. 33, DOI 10.1109/tpwrd.2017.2756831, no. 5, pp. 2106–2114, Oct. 2018.

[20] B. Li, M. Lv, B. Li, S. Xue, and W. Wen, "Research on an improved protection principle based on differential voltage traveling wave for VSC-HVDC transmission lines," *IEEE Transactions on Power Delivery*, vol. 35, DOI 10.1109/tpwrd.2020.2966267, no. 5, pp. 2319–2328, Oct. 2020.

[21] T. Lan, Y. Li, and X. Duan, "High fault-resistance tolerable traveling wave protection for multi-terminal VSC-HVDC," *IEEE Transactions on Power Delivery*, vol. 36, DOI 10.1109/tpwrd.2020.2998158, no. 2, pp. 943–956, Apr. 2021.

[22] R. Dantas, J. Liang, C. Ugalde-Loo, A. Adamczyk, C. Barker, and R. Whitehouse, "Protection strategy for multi-terminal DC networks with fault current blocking capability of converters," in *13th IET International Conference on AC and DC Power Transmission (ACDC 2017)*, DOI 10.1049/cp.2017.0021. Institution of Engineering and Technology, 2017.

[23] G. Auran, J. Descloux, S. Nguefeu, and B. Raison, "Non-unit full selective protection algorithm for MTDC grids," in *2017 IEEE Power & Energy Society General Meeting*, DOI 10.1109/pesgm.2017.8274087. Chicago, IL, USA, Jul. 2017.

[24] D. Tzelepis, A. Dysko, G. Fusiek, J. Nelson, P. Niewczas, D. Vozikis, P. Orr, N. Gordon, and C. D. Booth, "Single-ended differential protection in MTDC networks using optical sensors," *IEEE Transactions on Power Delivery*, vol. 32, DOI 10.1109/tpwrd.2016.2645231, no. 3, pp. 1605–1615, Jun. 2017.

[25] G. Song, T. Wang, and K. S. Hussain, "DC line fault identification based on pulse injection from hybrid HVDC breaker," *IEEE Transactions on Power Delivery*, vol. 34, DOI 10.1109/tpwrd.2018.2865226, no. 1, pp. 271–280, Feb. 2019.

[26] L. Liu, Z. Liu, M. Popov, P. Palensky, and M. A. M. M. van der Meijden, "A fast protection of multi-terminal HVDC system based on transient signal detection," *IEEE Transactions on Power Delivery*, vol. 36, DOI 10.1109/tpwrd.2020.2979811, no. 1, pp. 43–51, Feb. 2021.

[27] C. Zhang, G. bing Song, S. Meliopoulos, and X. Dong, "Setting-less non-unit protection method for DC line faults in VSC-MTDC systems," *IEEE Transactions on Industrial Electronics*, DOI 10.1109/tie.2021.3050380, pp. 1–1, 2021.

[28] J. Yang, J. E. Fletcher, and J. O'Reilly, "Multiterminal DC wind farm collection grid internal fault analysis and protection design," *IEEE Transactions on Power Delivery*, vol. 25, DOI 10.1109/tpwrd.2010.2044813, no. 4, pp. 2308–2318, Oct. 2010.

[29] J. Suonan, J. Zhang, Z. Jiao, L. Yang, and G. Song, "Distance protection for HVDC transmission lines considering frequency-dependent parameters," *IEEE Transactions on Power Delivery*, vol. 28, DOI 10.1109/tpwrd.2012.2232312, no. 2, pp. 723–732, Apr. 2013.

[30] V. A. Lacerda, R. M. Monaro, D. Campos-Gaona, D. V. Coury, and O. Anaya-Lara, "Distance protection algorithm for multiterminal HVDC systems using the hilbert–huang transform," *IET Generation, Transmission & Distribution*, vol. 14, DOI 10.1049/iet-gtd.2019.1551, no. 15, pp. 3022–3032, Aug. 2020.

[31] W. Leterme, P. Tielens, S. D. Boeck, and D. V. Hertem, "Overview of grounding and configuration options for meshed HVDC grids," *IEEE Transactions on Power Delivery*, vol. 29, DOI 10.1109/tpwrd.2014.2331106, no. 6, pp. 2467–2475, Dec. 2014.

[32] N. Ahmed, L. Ängquist, S. Mahmood, A. Antonopoulos, L. Harnefors, S. Norrga, and H.-P. Nee, "Efficient modeling of an MMC-based multiterminal DC system employing hybrid HVDC breakers," *IEEE Transactions on Power Delivery*, vol. 30, DOI 10.1109/tpwrd.2015.2398825, no. 4, pp. 1792–1801, Aug. 2015.

[33] M. K. Bucher and C. M. Franck, "Analytic approximation of fault current contribution from AC networks to MTDC networks during pole-to-ground faults," *IEEE Transactions on Power Delivery*, vol. 31, DOI 10.1109/tpwrd.2015.2401056, no. 1, pp. 20–27, Feb. 2016.

[34] W. Leterme, J. Beerten, and D. V. Hertem, "Equivalent circuit for half-bridge MMC DC fault current contribution," in *2016*

IEEE International Energy Conference (ENERGYCON), DOI 10.1109/energycon.2016.7513914, Leuven, Belgium, 2016.

[35] Y. Song, J. Sun, M. Saeedifard, S. Ji, L. Zhu, and A. P. S. Meliopoulos, "Optimum selection of circuit breaker parameters based on analytical calculation of overcurrent and overvoltage in multiterminal HVDC grids," *IEEE Transactions on Industrial Electronics*, vol. 67, DOI 10.1109/tie.2019.2921279, no. 5, pp. 4133–4143, May. 2020.

[36] C. Li, C. Zhao, J. Xu, Y. Ji, F. Zhang, and T. An, "A pole-to-pole short-circuit fault current calculation method for DC grids," *IEEE Transactions on Power Systems*, vol. 32, DOI 10.1109/tpwrs.2017.2682110, no. 6, pp. 4943–4953, Nov. 2017.

[37] H. Ye, S. Gao, G. Li, and Y. Liu, "Efficient estimation and characteristic analysis of short-circuit currents for MMC-MTDC grids," *IEEE Transactions on Industrial Electronics*, vol. 68, DOI 10.1109/tie.2020.2965433, no. 1, pp. 258–269, Jan. 2021.

[38] Y. Luo, J. He, M. Li, D. Zhang, Y. Zhang, Y. Song, and M. Nie, "Analytical calculation of transient short-circuit currents for MMC-based MTDC grids," *IEEE Transactions on Industrial Electronics*, DOI 10.1109/tie.2021.3099235, pp. 1–1, 2021.

[39] C. Christopoulos and A. Wright, *Electrical Power System Protection*. Springer US, 1999.

[40] S. H. Horowitz and A. G. Phadke, *Power System Relaying*, 3rd ed. John Wiley & Sons, Ltd, Apr. 2008.

[41] M. H. J. Bollen and I. Y.-H. Gu, *Signal Processing of Power Quality Disturbances*. John Wiley & Sons, Inc., Jul. 2006.

[42] V. A. Lacerda, P. Barbalho, R. Monaro, and D. Coury, "Signal processing techniques for synchrophasors considering short-circuit signals: A comparative study," *IET Generation, Transmission & Distribution*, DOI 10.1049/iet-gtd.2020.0208, May. 2020.

[43] M. D. Kusljevic, "On LS-based power frequency estimation algorithms," *IEEE Transactions on Instrumentation and Measurement*, vol. 62, DOI 10.1109/tim.2013.2248254, no. 7, pp. 2020–2028, Jul. 2013.

[44] W. Leterme, N. Ahmed, D. V. Hertem, J. Beerten, S. Norrga, and L. Ängquist, "A new HVDC grid test system for HVDC grid dynamics and protection studies in EMT-type software," in *11th IET International Conference on AC and DC Power Transmission*, DOI 10.1049/cp.2015.0068, Birmingham, UK, 2015.

[45] U. N. Gnanarathna, A. M. Gole, and R. P. Jayasinghe, "Efficient modeling of modular multilevel HVDC converters (MMC) on electromagnetic transient simulation programs," *IEEE Transactions on Power Delivery*, vol. 26, DOI 10.1109/tpwrd.2010.2060737, no. 1, pp. 316–324, Jan. 2011.

[46] V. A. Lacerda, R. M. Monaro, D. Campos-Gaona, D. V. Coury, and O. Anaya-Lara, "Distance protection algorithm for multiterminal HVDC systems using the hilbert–huang transform," *IET Generation, Transmission & Distribution*, vol. 14, DOI 10.1049/iet-gtd.2019.1551, no. 15, pp. 3022–3032, Aug. 2020.

[47] Y. Song, J. Sun, M. Saeedifard, S. Ji, L. Zhu, A. P. S. Meliopoulos, and L. Graber, "Reducing the fault-transient magnitudes in multiterminal HVdc grids by sequential tripping of hybrid circuit breaker modules," *IEEE Transactions on Industrial Electronics*, vol. 66, DOI 10.1109/tie.2018.2881941, no. 9, pp. 7290–7299, Sep. 2019.

Vinícius A. Lacerda (S'18) received a B.Sc. and PhD in Electrical Engineering from the University of São Paulo, São Carlos, Brazil in 2015 and 2021. He was a Visiting Researcher at the University of Strathclyde from 2018 to 2019. He is presently a Post-Doctorate researcher at the Universitat Politècnica de Catalunya, Spain. His areas of research interest are power systems modelling, short-circuit analysis and protection.

Renato M. Monaro (**S'10-M'13**) received the Ph.D. degree from the University of São Paulo, São Carlos, Brazil, in 2013. At present, he is an Assistant Professor at the University of São Paulo, São Paulo, Brazil. His main research interests include power system control and protection, HVDC-VSC transmission, distributed generation, and renewable energy.

Rafael Peña Alzola received the combined Licentiate and M.Sc. degree in industrial engineering from the University of the Basque Country, Bilbao, Spain, in 2001, and the Ph.D. degree in electrical engineering from the National University for Distance Learning, Madrid, Spain, in 2011.

He has worked as an Electrical Engineer for several companies in Spain. From September 2012 to July 2013, he was a Guest Postdoctoral Fellow with the Department of Energy Technology, Aalborg University, Aalborg, Denmark. From August 2014 to December 2016, he was Postdoctoral Research Fellow with the Department of Electrical and Computer Engineering, The University of British Columbia, Vancouver, BC, Canada. From January 2017 to May 2017, he was with the University of Alcala, Madrid, for a short-term industrial collaboration. Since June 2017, he has been a Research Fellow with the Rolls Royce University Technology Centre, University of Strathclyde, Glasgow, U.K. His research interests include energy storage, LCL filters, solid-state transformers, power electronics for hybrid electric aircraft, and innovative control techniques for power converters.

David Campos-Gaona (**M'12–SM'19**) received the B.E. degree in electronic engineering, and the M.Sc. and Ph.D. degrees in electrical engineering, all from Instituto Tecnolgico de Morelia, Morelia, Mexico, in 2004, 2007, and 2012, respectively.

From 2014 to 2016, he was a Postdoctoral Research Fellow with the Department of Electrical and Computer Engineering, University of British Columbia, Vancouver, BC, Canada. Since August 2016, he has been with the University of Strathclyde, Glasgow, U.K, first as a research associate and currently as Lecturer. His research interests include wind farm power integration, HVdc transmission systems, variable frequency systems, and real-time digital control of power-electronic-based devices.

Denis V. Coury received a B.Sc. degree in Electrical Engineering from the Federal University of Uberlândia, Brazil in 1983, an M.Sc degree from EESC - University of São Paulo, Brazil in 1986 and a PhD degree from Bath University, England in 1992. He worked for the Technological Research Institute (IPT), São Paulo, Brazil from 1985 to 1986. He joined the Department of Electrical and Computer Engineering, University of São Paulo, São Carlos, Brazil, in 1986, where he is presently a Full Professor in the Power Systems Group. Prof. Coury spent his Sabbatical at Cornell University (USA) during 1999-2000. His areas of research interest are power system protection, expert systems and Smart Grids.